JOURNAL OF GEOPHYSICAL RESEARCH, VOL. 90, NO. A8, PAGES 7449–7456, AUGUST 1, 1985

Analysis of 16 Plasma Vortex Events in the Geomagnetic Tail

J. BIRN, E. W. HONES, JR., AND S. J. BAME

Los Alamos National Laboratory, University of California, Los Alamos, New Mexico

C. T. RUSSELL

Institute of Geophysics and Planetary Physics, University of California, Los Angeles

The analysis of 16 plasma vortex occurrences in the magnetotail plasma sheet of Hones et al. (1983) is extended. We used two- and three-dimensional plasma measurements and three-dimensional magnetic field measurements to study phase relations, energy propagation, and polarization properties. The results point toward an interpretation as a slow strongly damped MHD eigenmode which is generated by tailward traveling perturbations at the low-latitude interface between plasma sheet and magnetosheath.

INTRODUCTION

As revealed by plasma data from ISEE 1 and 2 [*Hones et al.*, 1978], the nightside plasma sheet often exhibits wave modes that are characterized by rotations of the plasma bulk flow vector primarily in the equatorial plane. These waves have periods of typically 10 min and are strongly damped or quenched. No more than five rotations were ever observed during one event. The events were called vortex events because the waves were believed to be caused by transient large-scale vortices generated by shear flow, most likely at the magnetopause [*Hones et al.*, 1981]. A statistical survey of about 170 events [*Hones et al.*, 1981] showed that they occur across the entire tail within the range up to about 20 R_E covered by the ISEE satellites. The sense of rotation in the equatorial plane changes from clockwise as viewed from above the dawnside to anticlockwise on the duskside, and their occurrence is apparently independent of geomagnetic activity. The vortex events are relatively rare (only $\sim$170 events in 19 months). This result, however, might be due to the fact that only events with complete rotations of the total flow velocity were included in the study of *Hones et al.* [1981]. Events with smaller wave amplitudes that would lead only to a wavy deflection of the total flow vector could indeed be more frequent. There is no obvious correlation between the occurrence frequency and the distance from the magnetopause except that the occurrence seems to be less frequent near the midnight region. The waves have magnetic perturbations associated with them [*Saunders et al.*, 1981; *Saunders*, 1982; *Hones et al.*, 1983] and can sometimes be related to long-period (Pc 5) waves in ground magnetic field measurements [*Hones et al.*, 1981; *Saunders*, 1982; *Saunders et al.*, 1983*a*, *b*].

The wave signals are always observed at both ISEE satellites and show a high degree of correlation, as illustrated by Figure 1. It shows the longitude of the plasma flow and the x component of the magnetic field at ISEE 1 and 2 during a vortex event on March 2, 1978 (event 6 of Table 1) when the satellites were at X_{SE}, Y_{SE}, $Z_{SE} = -10.5, -10.0, +5.1$ R_E with a separation vector from ISEE 2 to ISEE 1, $\Delta r_{SE} = -945, -329, +388$ km. The period of rotation was $\sim$8 to 10 min. The determination of phase lags between the signals at ISEE 1 and ISEE 2 for this and 15 other events [*Hones et al.*, 1981, 1983] indicated wavelengths of about 5–30 R_E and phase speeds of 70–400 km/s.

On the other hand, anisotropies of energetic particles, interpreted as due to wave-associated density gradients, implied a shorter wavelength of about 5000 km, at least for one event [*Saunders et al.*, 1983*a*]. *Saunders et al.* [1983*b*] also concluded a wavelength of $\sim$8500 km for another event on the basis of the observed phase lag between ISEE 1 and 2 and of an assumed wave propagation perpendicular to the average magnetic field and to the main magnetic field perturbation.

The two largely different wavelength estimates need not necessarily be inconsistent, as the phase lag measurements yield only upper limits of wavelength and phase speed which can be much larger than the actual values for wave propagation close to perpendicular to the satellite separation vector. Whereas it is very unlikely that the two satellites were closely aligned with the wave front in every case, it is possible that this was the case for the events on the early morningside studied by Saunders et al. Note that for these locations the satellite trajectories and thus their separation vectors are roughly radial and aligned with the major magnetic field direction. This interpretation would imply a very large variation of the wavelength perpendicular to the magnetic field from $\sim$5000 km near the morningside to 7–30 R_E in the more distant tail.

In this paper we will present results from an extended and completed analysis of macroscopic plasma and magnetic field data for 16 vortex events discussed earlier by *Hones et al.* [1983] (hereinafter referred to as paper 1). As the large scale in space and time of the vortex events clearly points to an interpretation as MHD waves [*Saunders*, 1982], such a data analysis forms the basis for any interpretation. It is desirable, however, to include at some later time also energetic particle data from more than just one event to resolve the apparent discrepancy in wavelength estimates.

DATA ANALYSIS

Our analyses comprised three types of treatments of the data: The first was cross-correlation analyses of the two-dimensional plasma flows and the three-dimensional magnetic field data to measure the intersatellite phase lags of the wave signals. Most of the results are reported already in paper 1. The second type of treatment was various calculations of combined three-dimensional plasma and field data from a single

Paper number 4A8434.
0148-0227/85/004A-8434$05.00

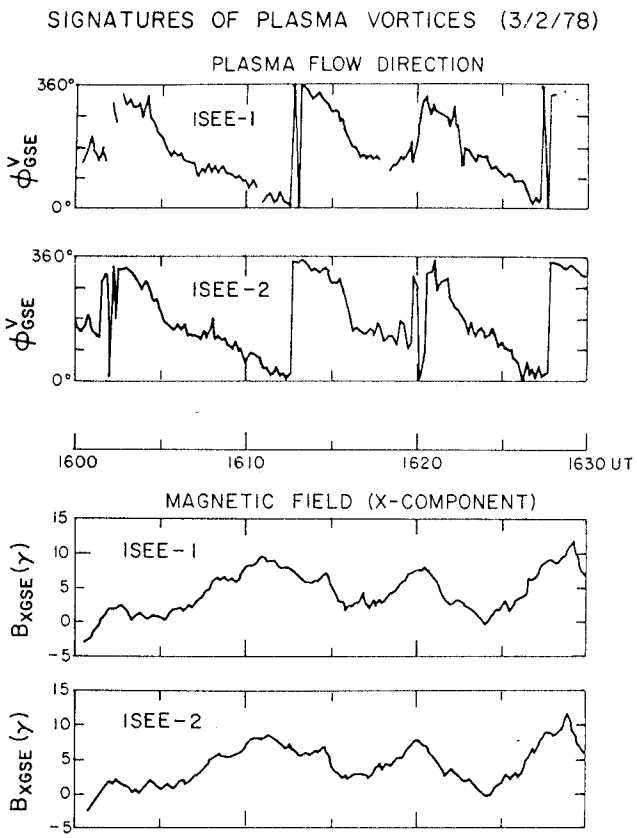

Fig. 1. Variations in the longitude of plasma flow and in the x component of the magnetic field measured simultaneously at ISEE 1 and 2 during a plasma vortex encounter on March 2, 1978 (event 6).

satellite (usually ISEE 2) to determine wave characteristics such as parallel and perpendicular (to **B**) flow components, electric field, and wave energy propagation characteristics. The third type of treatment was Fourier analyses of plasma pressure, density, and the velocity and magnetic field components. The main purpose was to get the phase relations of the plasma and field quantities which are important for a local wave analysis. In addition we can get the same information as from analyses 1 and 2, however, for each single Fourier component. It is also an easy way to find the polarization properties for velocity and magnetic field perturbations.

Results

Cross-Correlation Analysis

The basic results of the intersatellite cross-correlation analyses were already reported in paper 1. They were based on the calculation of cross-correlation coefficients for different time lags between the signals at the two ISEE satellites in each case. A parabola was fitted to the largest values of cross correlation to find the maximum K_{max} and the corresponding time lag which was used to determine the phase difference and therefrom phase speed and wavelength. The results indicate wavelengths of $\sim$5–30 R_E and phase speeds of $\sim$70 to a few hundreds of kilometers per second. These values, however, are maximum values in each case, as the intersatellite phase lags yield only the wave vector component and thereby the apparent velocity along the satellite separation direction, rather than the phase velocity along the wave normal. The actual values are expected to be smaller on the average by a factor of order $\frac{1}{2}$. The phase lags were also found to be variable in time and to differ somewhat for different components of **v** and **B**, although they generally agreed. For a more detailed representation and discussion we refer to that paper and in particular to their Table 1.

An additional piece of information, which was not yet reported, can be obtained from the magnitude of the cross-correlation coefficients K_{max} for each event. If the vortex waves are interpreted in terms of wave turbulence, the magnitude of K_{max} provides an estimate of the coherence length L of the wave signals. For isotropic turbulence the correlation coefficient K should fall off with distance $\Delta\mathbf{r}$ according to

$$K = \exp(-|\Delta\mathbf{r}|/L) \quad (1)$$

Of course, the vortex waves probably do not fulfill the assumption of isotropic turbulence, but equation (1) might still serve as a rough estimate of the coherence length L. Table 1

TABLE 1. Results From Intersatellite Phase Lags

Event	Date	Time Interval for Correlation Analysis	Satellite Separation $\lvert\Delta\mathbf{r}\rvert$, km	Upper Limit of Phase Speed c_{max}, km/s	Upper Limit of Wavelength λ_{max}, R_E	Maximum Correlation Coefficient K_{max}	Coherence Length L, R_E
1	Dec. 9, 1977	1454–1528	697	107	12.1	0.970	3.6
2	Dec. 11, 1977	2310–2323	848	4,000	240	0.971	4.5
3	Dec. 19, 1977	0435–0500	773	69	7.1	0.909	1.3
4	Dec. 28, 1977	1720–1745	939	81	7.6	0.982	8.2
5	March 2, 1978	1430–1450	944	137	14.2	0.909	1.6
6	March 2, 1978	1603–1627	1073	238	22.4	0.903	1.6
7	June 18, 1978	0510–0544	1165	243	22.8	0.931	2.6
8	June 25, 1978	0730–0757	1155	263	17.3	0.965	5.1
9	Jan. 5, 1979	1918–2000	5055	190	16.1	0.568	1.4
10	Jan. 30, 1979	1500–1545	2641	26,000	3,000	0.796	1.8
11	Feb. 11, 1979	0820–0840	2425	674	63	0.726	1.2
12	Feb. 11, 1979	0900–0915	2415	456	33.4	0.697	1.0
13	Feb. 11, 1979	1220–1250	2648	250	31	0.905	4.2
14	Feb. 11, 1979	1510–1530	3133	209	19.6	0.530	0.8
15	Feb. 22, 1979	1927–1954	5361	190	10.1	0.751	2.9
16	March 10, 1979	1130–1230	9481	315	35.5	0.750	5.2
17	Feb. 6, 1978	0230–0430	228	...	...	0.638	0.08

TABLE 2. Average Parameters of the Vortex Events (ISEE 2)

Event	B_x	B_y, nT	B_z	$\bar{n}$, cm^{-3}	β	v_A, km/s	v_S, km/s	a_i, km
1	14.1	39.9	10.2	1.36	0.32	755	390	118
2	25.9	61.5	−0.8	0.83	0.41	1145	665	219
3	7.4	29.5	5.3	1.04	0.58	595	410	190
4	34.9	36.0	13.0	1.13	0.55	975	655	173
5	18.8	12.8	0.1	0.43	1.37	630	670	497
6	4.0	2.4	3.7	0.44	22.1	160	695	1950
7	13.9	−8.2	7.1	1.14	2.32	315	440	371
8	11.5	−10.5	8.5	0.65	1.64	475	555	358
9	0.7	4.3	9.0	0.46	8.01	185	480	1640
10	−2.3	0.1	11.4	0.47	3.98	280	505	875
11	−2.6	5.4	7.0	1.67	7.76	80	195	975
12	1.6	5.5	4.7	1.26	15.5	75	265	1560
13	1.5	4.7	8.1	0.63	5.36	175	370	990
14	5.1	6.8	11.9	1.36	1.36	205	220	301
15	3.3	5.9	12.1	1.49	9.46	145	405	975
16	−23.1	−15.4	19.2	0.87	1.16	335	325	627

lists in addition to the phase speeds and wavelengths of paper 1 the values of K_{max} and the corresponding values of L according to (1). We used K_{max} derived from either **v** or **B**, whichever showed better correlations. The way in which the values of K_{max} are calculated is described in detail in paper 1. The interpretation is complicated by the fact that the total perturbation consists not only of the main wave signal but probably of several additional signals belonging to shorter time and length scales. If we assume that a perturbation consisted of two independent signals with two different coherence lengths L_1 and L_2, the coherence length L calculated from (1) lies between L_1 and L_2, approaching the longer one for longer separation distances. For comparison, we calculated the maximum cross-correlation coefficient for an interval of fluctuating flow that was not a vortex event (February 6, 1978, 0230–0430 UT, event 17). The value of K_{max} was 0.638 for a satellite separation distance of only 228 km, leading to a coherence length of only 500 km. If we assume that such kind of "noise" is present also during the vortex events, we see that the vortex wave signals are probably coherent over distances larger than the ~ 1 to 5 R_E given in Table 1. Coherence therefore probably exists over roughly one vortex wavelength. Without results for much longer satellite separations we cannot decide, however, whether two or more coherent vortices are present in the tail at the same time.

Local Analysis

A local analysis using the combined three-dimensional plasma and magnetic field data was done to get additional information on the character of the waves. The magnetic data, which were available at higher time resolution than the plasma data, were averaged over the same time intervals used to collect the plasma data. Tables 2 and 3 list some of the results. The wave amplitudes that are not included in the tables range typically between 50 and 100 km/s for the major velocity perturbation and 2–6 nT for the major magnetic field perturbation. Only ISEE 2 data are presented because no three-dimensional ISEE 1 data exist from January 1979 on and because ISEE 1 data were usually of poorer quality than ISEE 2 data before that date. Table 2 gives some background information on the average magnetic field, particle density, the parameter β equal to the ratio of the average plasma pressure p_0 and the magnetic pressure, the Alfvén velocity V_A, the sound speed defined by $V_s = (\gamma p_0/\rho_0)^{1/2}$ using $\gamma = \frac{5}{3}$, and the

TABLE 3. Flow and Energy Propagation Properties (ISEE 2)

	Average Flow Perturbations, km/s			Wave Energy Fluxes, μW/m^2										
Event	$\hat{v}_\parallel$	$\hat{v}_\perp$	$\hat{v}$	S_x	S_y	S_z	T_x	T_y	T_z	R_x	R_y	R_z	F_x	F_y	F_z
1	23.0	31.0	49.5	−0.43	3.55	−2.19	−0.22	1.09	−0.55	0.04	−0.05	0.03	−0.60	4.59	−2.71
2	49.5	54.4	91.5	−26.3	25.7	−34.0	4.05	3.89	2.31	−0.04	−0.01	−0.05	−22.3	29.6	−31.7
3	17.9	21.0	34.7	0.29	0.05	0.55	−0.06	−0.06	−0.17	−0.003	0.000	−0.002	0.23	−0.01	0.39
4	23.2	33.4	53.5	−1.87	5.46	−8.05	1.97	−0.13	1.54	0.01	−0.03	0.05	0.12	5.29	−6.46
5	49.5	51.5	88.1	−1.58	3.36	−0.99	−0.86	−1.05	1.14	−0.02	0.01	−0.01	−2.46	2.32	0.15
6	40.2	64.0	99.0	−0.57	0.12	−0.21	1.73	−1.92	1.75	0.004	−0.03	0.02	1.17	−1.83	1.56
7	17.8	27.4	42.6	0.002	0.12	0.20	−0.58	−1.59	0.38	0.001	−0.01	0.002	−0.58	−1.47	0.58
8	30.8	37.8	61.7	−1.28	−0.99	1.94	−1.36	1.10	−0.14	−0.04	−0.02	0.04	−2.69	0.09	1.85
9	17.1	41.4	61.0	0.32	−0.42	0.12	0.80	−0.20	0.06	0.03	0.01	0.01	1.14	−0.61	0.19
10	17.2	71.8	103.0	−1.28	−0.63	−2.41	−4.02	−0.24	3.74	0.19	−0.02	−0.13	−5.11	−0.89	1.21
11	39.5	52.6	84.2	−0.89	2.64	−0.07	−1.99	−2.07	6.83	−0.12	0.06	0.04	−2.99	0.63	6.80
12	21.0	33.0	51.2	0.81	1.15	1.33	−0.60	−0.05	0.45	−0.01	−0.01	0.01	0.21	1.09	1.80
13	14.7	33.2	49.2	−0.21	−0.15	0.19	−0.12	0.09	−0.13	0.003	0.001	0.008	−0.32	−0.06	0.06
14	26.0	51.7	77.6	−0.99	0.61	0.52	−1.01	−0.16	0.02	0.13	0.14	−0.09	−1.87	0.59	0.45
15	13.7	52.8	75.9	−3.33	−1.36	−4.25	−5.00	3.51	−0.52	0.15	−0.05	0.05	−8.18	2.11	−4.72
16	36.8	50.6	80.5	−2.64	5.22	−0.69	1.02	1.75	−5.51	0.04	−0.06	0.03	−1.58	6.91	−6.16

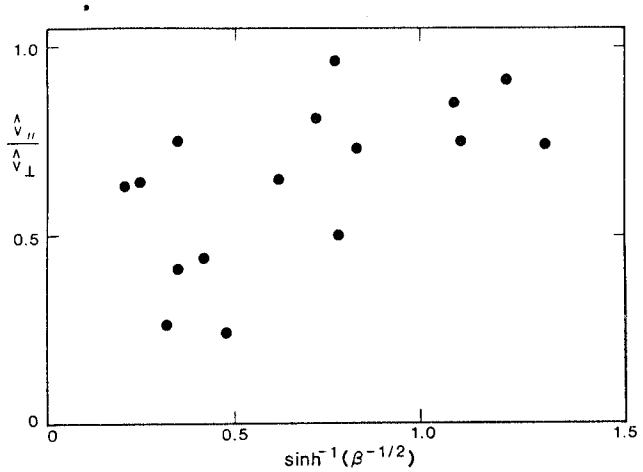

Fig. 2. Distribution of the ratio of the velocity perturbations parallel and perpendicular to the average magnetic field within the plasma sheet as indicated by $\zeta = \text{arcsinh } \beta^{-1/2}$.

proton Larmor radius a_i, calculated from the average magnetic field and the thermal speed. The ISEE 2 plasma data were calculated from the count rates using the Lockheed composition measurements on ISEE 1 (courtesy of W. Lennartsson).

The magnetic field values and in particular the values of β show clearly that the waves occur throughout the entire plasma sheet and are not, for instance, a phenomenon of the boundary layer between plasma sheet and lobe which is often found to be a region of strong flows [*Lui et al.*, 1977; *Forbes et al.*, 1981; *Eastman et al.*, 1984]. Also, the fact that no event was observed by one satellite and not by the other shows that the vortex waves are not restricted to narrow sheets within the plasma sheet but rather involve large volumes of it.

The phase speeds calculated from the intersatellite phase lags as given in Table 1 are typically below Alfvén and sound speed even though the phase speed values represent upper limits. The few cases where c_{max} lies above V_A and V_s can easily be attributed to a phase propagation close to perpendicular to the satellite separation vector. On the other hand, since it is unlikely that such a propagation direction occurred in all events, the true wavelengths lie probably not much below the minimum value of λ_{max}, which is still much larger than a proton Larmor radius. It is therefore unlikely that the waves are generally kinetic Alfvén waves, which in principle can also generate rotating flow directions.

The first three columns of Table 3 give the rms values of the total perturbation velocity $\mathbf{v}_1$ and of the components parallel and perpendicular to the average magnetic field $\mathbf{B}_0$ defined by

$$\hat{v} = \langle v_1^2 \rangle^{1/2} \tag{2}$$

$$\hat{v}_{\parallel} = \langle (\mathbf{v}_1 \cdot \mathbf{B}_0)^2 / B_0^2 \rangle^{1/2} \tag{3}$$

$$\hat{v}_{\perp} = \langle (\mathbf{v}_1 \times \mathbf{B}_0)^2 / 2B_0^2 \rangle^{1/2} \tag{4}$$

For a better comparison with $\hat{v}_{\parallel}$ the values of $v_{\perp}^2$ are divided by 2, since two components contribute to $\hat{v}_{\perp}$. Although $\hat{v}_{\parallel}$ is smaller than $\hat{v}_{\perp}$ in every case, there is obviously a significant part of the wave flow along the magnetic field in most cases. Figure 2 shows the distribution of $\hat{v}_{\parallel}/\hat{v}_{\perp}$ using $\zeta = \sinh^{-1}(\beta^{-1/2})$ as a rough measure of the distance from the neutral sheet (in a plane "Harris" sheet of the form $B_x = B_0 \tanh(z/L)$, ζ would correspond exactly to z/L). We can see a tendency of $\hat{v}_{\parallel}/\hat{v}_{\perp}$ to increase with increasing distance from the neutral sheet. This is consistent with the wave motion being mostly perpendicular to $\mathbf{B}$ in the neutral sheet and being converted into an increasing amount of parallel motion as the field direction changes into a direction more parallel to the ecliptic plane.

The distribution of flow perturbations $\hat{v}$ does not show any obvious correlation with the location in x, y, or z.

The next columns in Table 3 give the different contributions to the wave energy flux. If we ignore heat conduction there are three different contributions to the total energy flux density: the Poynting flux,

$$\mathbf{S} = -\frac{1}{\mu_0}(\mathbf{v} \times \mathbf{B}) \times \mathbf{B} = \frac{1}{\mu_0}(B^2\mathbf{v} - \mathbf{B} \cdot \mathbf{v}\mathbf{B}) \tag{5}$$

the enthalpy flux,

$$\mathbf{T} = (p + u)\mathbf{v} \tag{6}$$

where $u = \frac{3}{2}p$ represents the internal (here thermal) energy density, and the kinetic energy flux,

$$\mathbf{R} = \tfrac{1}{2}\rho v^2 \mathbf{v} \tag{7}$$

In (5) we have used the ideal MHD condition of very high conductivity $\mathbf{E} + \mathbf{v} \times \mathbf{B} = 0$, and in (6) the isotropy of the pressure tensor. This isotropy is found to hold for the present events to within a few percent, as illustrated by Figure 3 for

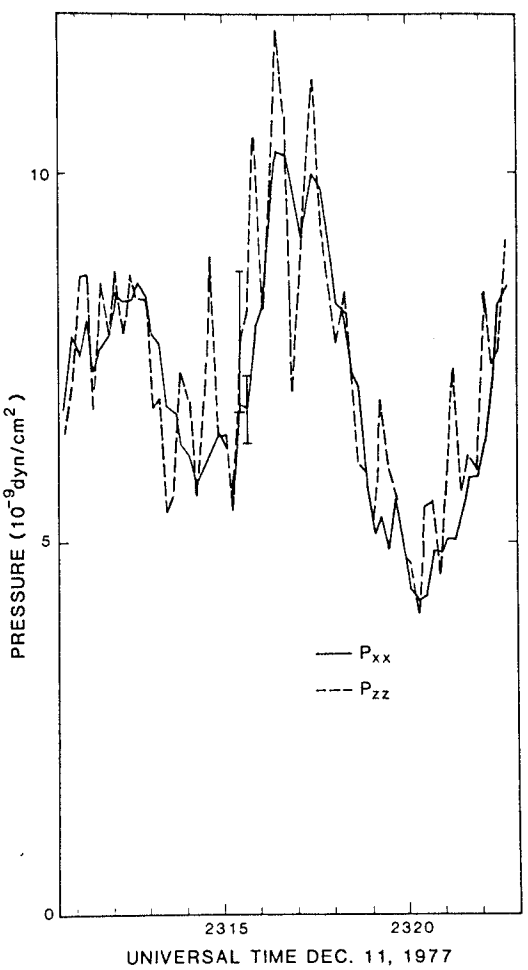

Fig. 3. Pressure tensor components P_{xx} and P_{zz} as a function of time for event 2. The two error bars indicate representative statistical errors due to finite count rate and the binning procedure. Note that P_{yy} agrees with P_{xx} to within the drawing accuracy.

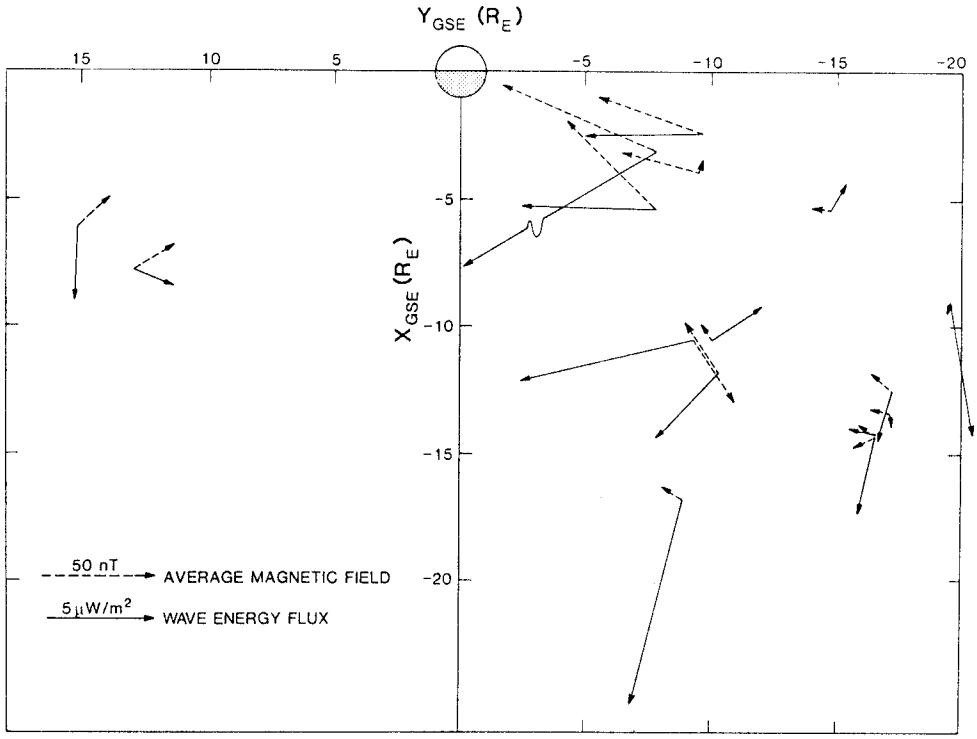

Fig. 4. Vectors of the average wave energy density **F** (solid arrows) and the average magnetic field (dashed arrows) of the individual vortex events as projected into the GSE x, y plane.

event 2. This figure shows the pressure tensor components P_{xx} and P_{zz}. The component P_{yy} agrees with P_{xx} to within the drawing accuracy of Figure 3. The larger deviations of P_{zz} reflect the lesser accuracy of this component and not a real anisotropy.

Here we are interested in those contributions to the energy flux that are due to the wave and give nonzero averages. It is obvious that these net values must be at least of second order in the perturbed quantities. The appropriate frame of reference to use (see, for example, *Anderson* [1963]) is the frame in which

$$\langle \rho \rangle = \rho_0 \tag{8}$$

$$\langle \rho \mathbf{v} \rangle = 0 \tag{9}$$

$$\langle \mathbf{B} \rangle = \mathbf{B}_0 \tag{10}$$

where the angle brackets again denote a time average and ρ_0 and $\mathbf{B}_0$ are values of density and magnetic field in the absence of the wave. If we define the perturbed quantities by

$$\rho_1 = \rho - \rho_0$$

$$\mathbf{v}_1 = \mathbf{v} - \mathbf{v}_0$$

where $\mathbf{v}_0 = 0$ in the chosen frame and

$$\mathbf{B}_1 = \mathbf{B} - \mathbf{B}_0$$

then we find that

$$\langle \rho_1 \rangle = 0$$

$$\langle \mathbf{B}_1 \rangle = 0$$

The velocity perturbation, however, has usually a nonvanishing average of second order, as can be found from (9):

$$\rho_0 \langle \mathbf{v}_1 \rangle = -\langle \rho_1 \mathbf{v}_1 \rangle \tag{11}$$

We find then the net wave energy flux contributions to lowest nonvanishing order:

$$\langle \mathbf{S} \rangle = \frac{1}{\mu_0} \langle B^2 \mathbf{v}_1 - \mathbf{B} \cdot \mathbf{v}_1 \mathbf{B} \rangle$$

$$= \frac{1}{\mu_0} \langle 2\mathbf{B}_0 \cdot \mathbf{B}_1 \mathbf{v}_1 - \mathbf{B}_0 \cdot \mathbf{v}_1 \mathbf{B}_1 - \mathbf{B}_1 \cdot \mathbf{v}_1 \mathbf{B}_0 \rangle$$

$$- \frac{1}{\mu_0 \rho_0} \langle {B_0}^2 \rho_1 \mathbf{v}_1 - \rho_1 \mathbf{B}_0 \cdot \mathbf{v}_1 \mathbf{B}_0 \rangle \tag{12}$$

$$\langle \mathbf{T} \rangle = \tfrac{5}{2} \langle p \mathbf{v}_1 \rangle$$

$$= \tfrac{5}{2} \langle p_1 \mathbf{v}_1 - p_0 (\rho_1 / \rho_0) \mathbf{v}_1 \rangle \tag{13}$$

$$\langle \mathbf{R} \rangle = \tfrac{1}{2} \langle \rho {\mathbf{v}_1}^2 \mathbf{v}_1 \rangle \tag{14}$$

Note the terms in (12) and (13) that result from (11).

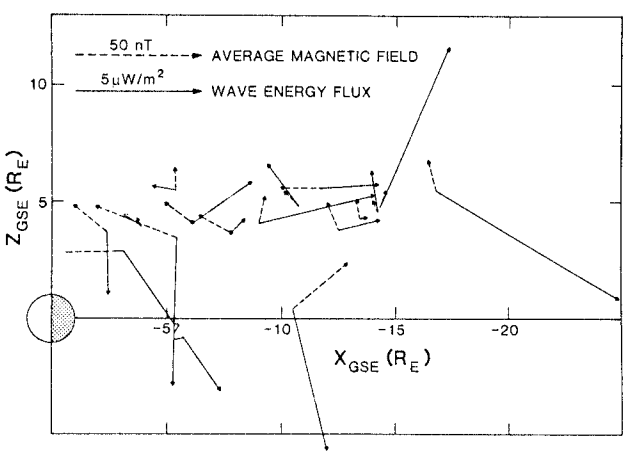

Fig. 5. The same as Figure 4, but projected into the GSE x, z plane.

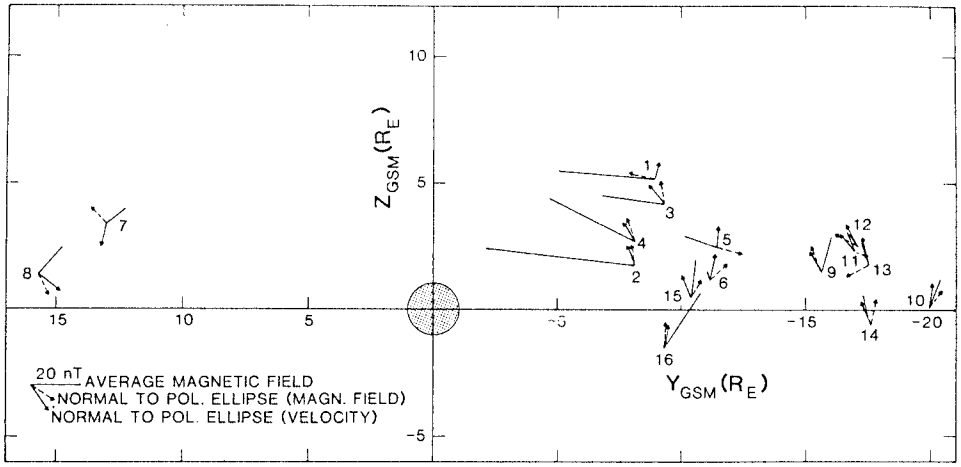

Fig. 6. Normals to the polarization ellipses of the magnetic field and plasma velocity perturbations projected onto the GSM y, z plane.

The kinetic energy flux given by (14) is of third order in the perturbed quantities or even smaller. It should therefore be much smaller than the other two contributions, which is confirmed by the values in Table 3. These three fluxes are summed and entered in the last three columns of Table 3.

The total flux density vectors are also shown in Figures 4 and 5 in two different projections along with the average magnetic field vectors. Figure 4 differs somewhat from the corresponding Figure 4 of paper 1 because the preliminary data evaluation contained an error. This error, however, did not alter the qualitative conclusions. The x components of the energy fluxes show clearly a dominance of antisunward flow. Only five of the 16 cases show weak sunward flow components. For three of these five events we have also ISEE 1 data available, two of which show instead antisunward flow, whereas all four cases of antisunward flow at ISEE 2, where ISEE 1 data exist, also show antisunward flow at ISEE 1.

In a similar way the y components show a dominance of inward flow away from the magnetopause toward the center of the tail. Again the cases of outward flow are less certain, as indicated by two opposite results from ISEE 1 of three available.

The z components of the total energy fluxes are predominantly directed away from the center of the plasma sheet with the remarkable exception of three events (1, 2, and 4) at similar locations on the morningside. One more case (event 15) with a z component toward the neutral sheet occurs relatively close to the neutral sheet as indicated by the large value of β and the comparably large B_z. This exception seems therefore less significant. This result did not show up in the preliminary data analysis which formed the basis of paper 1, because of the error mentioned above.

The calculation of field-aligned components shows that the preferred direction along the field is toward the earth.

In summary, the energy flow results point clearly toward a generating mechanism near the magnetopause at low latitudes, very likely a Kelvin-Helmholtz instability at the magnetopause or low-latitude boundary layer.

Fourier Analysis

Selected periods of each of the events were used to do a Fourier analysis for each of the three-dimensional components of $\mathbf{v}_1$ and $\mathbf{B}_1$. Such an analysis enabled us to determine in an easy way the polarization ellipses and their orientation for each of the Fourier components of $\mathbf{v}_1$ and $\mathbf{B}_1$. Normals to the polarization ellipses of the basic Fourier component are shown in two different projections in Figures 6 and 7. The orientation of the normal follows a left-hand rule with respect to the sense of the rotating perturbation vectors such that the upward (in $+z$ direction) pointing normals on the dawnside correspond to clockwise rotation as viewed from above, whereas the downward pointing normals on the duskside (indicated by small circles in Figure 7) correspond to counterclockwise rotation. The orientation of the two normals calculated from $\mathbf{v}_1$ and $\mathbf{B}_1$ usually agrees well. The few exceptions belong to cases where either $\mathbf{v}_1$ or $\mathbf{B}_1$ did not show the basic period very well, so that the results from the Fourier analysis were not very reliable for that quantity. Projections of the polarization ellipses in the x, y plane are shown in Figure 8. Since the normals to these ellipses are mainly in the z direction, the ellipticity apparent from Figure 8 is usually close to the real value. The figure shows that in most cases the two ellipses calculated from $\mathbf{v}_1$ and $\mathbf{B}_1$ have similar orientation, with the magnetic field ellipse usually being more elongated (i.e., closer to linear polarization).

The Fourier analysis allows also an easy determination of phase relation between different components of $\mathbf{v}_1$ and $\mathbf{B}_1$. Since most of the observations are made in the dawn sector

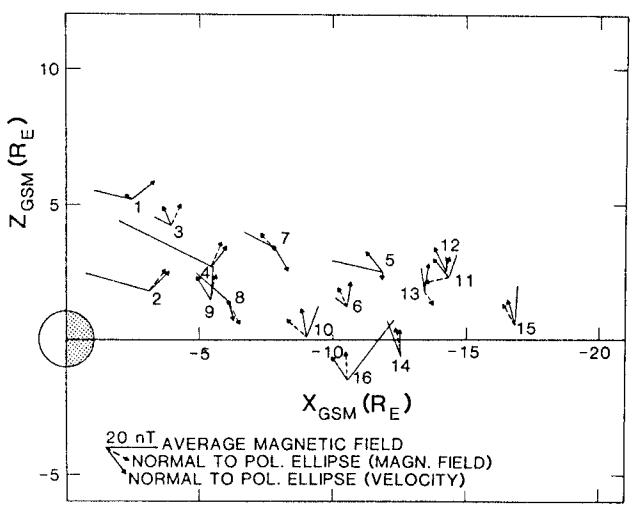

Fig. 7. The vectors in Figure 6 projected onto the GSM x, z plane. The two events with small circles at their origins are in the duskside of the tail.

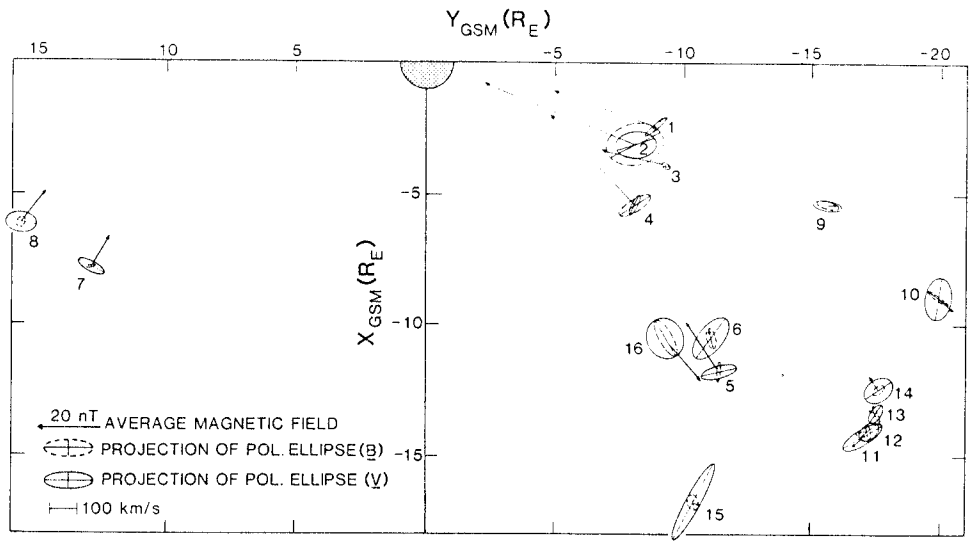

Fig. 8. Projections of the polarization ellipses of the magnetic perturbation and the velocity perturbation onto the GSM x, y plane. The two events in the dusk sector of the tail are not shown because their ellipses were too small to be drawn to this scale.

above the neutral sheet, we have, for better statistics, converted also the few observations outside this section into this sector using symmetry conditions. We find that on the average the magnetic perturbation vector in the ecliptic plane leads the velocity perturbation vector by about 103° in space with 11 of the 16 events between 75° and 155°. This is close to what one expects for perturbations that rotate closed magnetic flux tubes in a clockwise sense in the neutral sheet region while the ends of those flux tubes at the earth are fixed as illustrated by Figure 9.

The figure shows that for clockwise rotation of the flow and earthward orientation of the average field, one should expect to see the maximum stretching ($\mathbf{B}_1$ earthward) when the flow is duskward, dawnward perturbation of the magnetic field when the flow is earthward, and so on. That means one should indeed expect the magnetic field perturbation to lead the flow perturbation by about 90°.

The few cases that differ from this picture occurred close to the neutral sheet where the relation between flow and magnetic perturbations seems less predictable. For exact symmetry, B_{x_1} and B_{y_1} should actually vanish at the neutral sheet where $\mathbf{B}$ is in the z direction. The magnetic perturbations in x and y are indeed generally smaller (and less regular) for cases 9 to 15, which have their average magnetic field mostly in the z direction.

Additional results are as follows: The waves are usually accompanied by pressure and density perturbations mostly in phase with each other. Perturbations of magnetic and thermal plasma pressure are mostly close to antiphase. The cases with in-phase or close to $\pm 90°$ phase relations are again cases which occurred close to the neutral sheet.

Summary and Conclusions

The results of an extended data analysis of 16 vortex events described in this paper and our previous paper [*Hones et al.*, 1983] have led to the following major properties of these waves:

1. The vortex waves are large-scale events involving a large fraction of the plasma sheet and scale lengths of usually at least 5 R_E (although in individual cases a shorter wavelength cannot be excluded). There is no indication from plasma and field data that the scale lengths in x and y are generally largely different, and the scale size in the z direction is probably comparable to the plasma sheet thickness. It is not clear yet whether coherence of more than one vortex exists at one time. The wavelength seems to increase with distance down tail. The waves are not surface waves restricted, for example, to the transition layer between plasma sheet and lobe or to the vicinity of the magnetopause.

2. The energy propagation is predominantly tailward and inward, i.e., toward midnight. The field-aligned energy flux is predominantly toward the earth. These features point clearly toward a source mechanism operating near the low-latitude boundary layer or magnetopause. A likely candidate is a Kelvin-Helmholtz instability at the interface between plasma sheet and low-latitude boundary layer suggested earlier [*Hones et al.*, 1981].

3. The fact that the wave amplitudes and the occurrence frequency do not fall off as surface waves with increasing distance from the boundary indicates, however, that a large-scale resonance plays an important role also. This resonance is apparently not a single flux tube resonance determined by the length of a magnetic flux tube as is usually considered for dayside Pc 5 events, because the period of the vortex events is apparently independent of location and the vortex events involve larger fractions of the tail plasma sheet. For the occurrence of nightside Pc 5 waves in ground magnetic field measurements associated with the vortex waves such flux tubes resonances may, however, be important.

4. Even the upper limits of the phase speed obtained from intersatellite time lags are usually well below Alfvén and sound speed. This fact and the mostly antiphase variations of

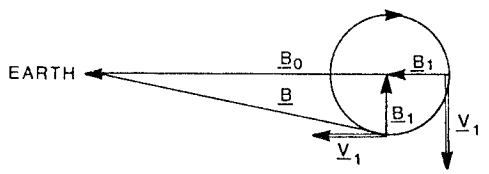

Fig. 9. Sketch of magnetic field changes to be expected for clockwise rotation of the flow on a field line that is fixed near the earth.

magnetic and thermal pressure favor an interpretation of the waves as slow MHD modes propagating in directions close to perpendicular to the magnetic field. One must be aware, however, that usual MHD wave theory and classification cannot be simply applied because of the long wavelength of the vortex waves which is comparable to or even larger than the typical equilibrium scale length, e.g., the thickness of the plasma sheet.

The combination of these results favors the following interpretation of the vortex waves: The waves are generated by perturbations at the low-latitude boundary near the magnetopause, probably through a Kelvin-Helmholtz instability. The large wavelength, however, seems to be the consequence of an additional resonant effect. Since the vortex waves differ from dayside Pc 5 pulsations, which seem to be more localized with resonances determined by the finite length of the resonant flux tube, it seems more likely that the wavelength and the period are determined by a different equilibrium scale size, for instance the finite width of the magnetotail in the y direction. The generation mechanism and the resonance would primarily determine the flow characteristics in the neutral sheet. The flow in the equatorial plane then drives the motion of closed magnetic field lines and also generates magnetic field perturbations in regions above and below the neutral sheet. The character of the waves is closest to that of slow MHD modes which propagate close to perpendicular to the magnetic field. Note that although the phase speed of slow MHD modes vanishes in the limit of perpendicular propagation (with the waves approaching the character of quasi-static oscillations), the group velocity, i.e., the energy propagation speed, stays finite. The fact that the equilibrium configuration is nonuniform with scale sizes comparable to the wavelength implies that the vortex waves cannot behave as pure MHD modes as derived in usual wave theory. Using a small perpendicular wavelength approximation, *Southwood and Saunders* [1985] have shown that it is the curvature of field lines near the neutral sheet that primarily leads to a coupling between slow MHD modes and Alfvén modes.

Unlike many dayside Pc 5 events the vortex waves consist only of very few wave periods. This indicates either a generating mechanism of relatively short duration or a strong damping or quenching of resonant waves. Possible damping mechanisms are Landau damping, which is known to be very strong for magnetoacoustic waves at high ion temperatures ($T_i \gtrsim T_e$), or a phase mixing process that operates in a nonuniform medium. The energy density in these waves is typically 2×10^{-11} ergs/cm^3, much smaller than the thermal energy. The total energy in a slab of $5 \times 20 \times 40$ $R_E{}^3$ would amount to $\sim 2 \times 10^{10}$ ergs. It is not clear where this energy is dissipated. The general energy flow direction tailward and toward midnight does not show a strong convergence into a dissipation region. This fact together with the short duration suggests that the energy is probably dissipated over a large body of the tail plasma sheet. Because of the rare occurrence of these events the dissipated energy cannot contribute significantly to the heating of the plasma sheet.

Acknowledgments. Work at Los Alamos was done under the auspices of the U.S. Department of Energy with NASA support under contract S-04039D. Work at UCLA was supported by NASA contract NAS-5-25772. We thank W. Lennartsson for providing the ion composition data from Lockheed measurements on ISEE 1. We thank also G. Paschmann as the principal investigator of the Los Alamos/Max Planck Institute plasma experiment on ISEE 2 for provision of the data.

The Editor thanks A. T. Y. Lui and C. Y. Huang for their assistance in evaluating this paper.

REFERENCES

Anderson, J. E., *Magnetohydrodynamic Shock Waves*, MIT Press, Cambridge, Mass., 1963.

Eastman, T. E., L. A. Frank, W. K. Peterson, and W. Lennartsson, The plasma sheet boundary layer, *J. Geophys. Res.*, *89*, 1553, 1984.

Forbes, T. G., E. W. Hones, Jr., S. J. Bame, J. R. Asbridge, G. Paschmann, N. Sckopke, and C. T. Russell, Evidence for the tailward retreat of a magnetic neutral line in the magnetotail during substorm recovery, *Geophys. Res. Lett.*, *8*, 261, 1981.

Hones, E. W., Jr., G. Paschmann, S. J. Bame, J. R. Asbridge, N. Sckopke, and K. Schindler, Vortices in magnetospheric plasma flow, *Geophys. Res. Lett.*, *5*, 2069, 1978.

Hones, E. W., Jr., J. Birn, S. J. Bame, J. R. Asbridge, G. Paschmann, N. Sckopke, and G. Haerendel, Further determination of the characteristics of magnetospheric plasma vortices with ISEE 1 and 2, *J. Geophys. Res.*, *86*, 814, 1981.

Hones, E. W., Jr., J. Birn, S. J. Bame, and C. T. Russell, New observations of plasma vortices and insights into their interpretation, *Geophys. Res. Lett.*, *10*, 674, 1983.

Lui, A. T. Y., E. W. Hones, Jr., F. Yasuhara, S.-I. Akasofu, and S. J. Bame, Magnetotail plasma flow during plasma sheet expansion: VELA 5 and 6 and IMP 6 observations, *J. Geophys. Res.*, *82*, 1235, 1977.

Saunders, M. A., Analysis of ISEE-1 and 2 spacecraft magnetometer data, thesis, Imp. Coll. of Sci. and Technol., London, 1982.

Saunders, M. A., D. J. Southwood, E. W. Hones, Jr., and C. T. Russell, A hydromagnetic vortex seen by ISEE-1 and 2, *J. Atmos. Terr. Phys.*, *43*, 927, 1981.

Saunders, M. A., D. J. Southwood, T. A. Fritz, and E. W. Hones, Jr., Hydromagnetic vortices, 1, The 11th December 1977 event, *Planet. Space Sci.*, *31*, 1099, 1983*a*.

Saunders, M. A., D. J. Southwood, and E. W. Hones, Jr., Hydromagnetic vortices, 2, Further dawnside events, *Planet. Space Sci.*, *31*, 1117, 1983*b*.

Southwood, D. J., and M. A. Saunders, Curvature coupling of slow and Alfvén MHD waves in a magnetotail field configuration, *Planet. Space Sci.*, *33*, 127, 1985.

S. J Bame, J. Birn, and E. W. Hones, Jr., Los Alamos National Laboratory, Los Alamos, NM 87545.

C. T. Russell, Institute of Geophysics and Planetary Physics, University of California, Los Angeles, CA 90024.

(Received December 3, 1984;
revised March 12, 1985;
accepted March 13, 1985.)